Heat conduction and energy relaxation in an InAs nanowire approaching the clean one-dimensional limit

Subhomoy Haldar,[1,2,*] Diego Subero,[3] Mukesh Kumar,[1] Bayan Karimi,[3,4] Adam Burke,[1] Lars Samuelson,[1,5] Jukka Pekola,[3] and Ville F. Maisi[1,†]

[1]*NanoLund and Solid State Physics, Lund University, Box 118, 22100 Lund, Sweden*
[2]*Department of Physics, Indian Institute of Technology Kanpur, Uttar Pradesh 208016, India*
[3]*Pico Group, QTF Centre of Excellence, Department of Applied Physics, Aalto University School of Science, P.O. Box 13500, 00076 Aalto, Finland*
[4]*Pritzker School of Molecular Engineering, University of Chicago, Chicago, Illinois 60637, USA*
[5]*Institute of Nanoscience and Applications, SUSTech, Shenzhen, China*

(Received 31 March 2026; revised 4 September 2026; accepted 19 October 2026; published 6 November 2026)

We investigate heat conduction and energy relaxation in an InAs semiconductor nanowire using a hybrid semiconductor-superconductor architecture. Local electronic temperatures are measured with an *insitu* grown quantum dot thermometer, while controlled Joule heating is applied at different locations along the wire to probe the heat flow along the nanowire at subkelvin temperatures. With a one-dimensional heat transport model, we calculate an electron-phonon heat flow that scales as $Q_{\text{e-ph}} \propto T^{2.6}$, which is in close agreement with the T^3 dependence predicted for clean one-dimensional phonons coupled to the electron gas. We further estimate a characteristic length $l_{\text{eq}} = 370$ nm; beyond this length scale, phonon-mediated heat transport dominates over heat conduction in our nanowire. Our results provide a quantitative measure of energy relaxation mechanisms in a one-dimensional semiconductor and provide a framework for studying heat flow in low-dimensional nanostructures.

DOI: 10.1103/g2cs-pdcw

I. INTRODUCTION

Heat conduction and energy dissipation in nanoscale systems play a central role in the performance of electronic, thermoelectric, and quantum devices [1–5]. At the heart of these devices, energy transport is determined by the electrical and thermal conductivity, phonon-assisted processes, and energy dissipation to the environment [6]. As the size of the system approaches the electronic mean free path and electron-phonon scattering length, energy transport depends on the quantized energy modes and mesoscopic effects [7–9]. A quantitative understanding of these regimes is essential for nanoscale thermoelectric devices, management of heat dissipation in cryogenic electronics, and mitigating decoherence in quantum circuits [2,10–12]. In particular, semiconductor nanowires (NWs) provide a platform for exploring energy transport at these length scales. Their one-dimensional geometry, high crystalline quality, and tunability of electronic transport by electrostatic gates help control charge and heat conduction independently [5,9,12]. In lower dimensions, phonon spectra are modified, boundary scattering becomes dominant, and cooling power laws can deviate substantially from the conventional T^5 dependence for ordinary metals [13–15]. Such deviations, together with violations of the Wiedemann-Franz law in nanoscale semiconductors and metals due to Coulomb effects [9,16] show a different thermal transport regime. Recent years have seen rapid progress in the study of heat conduction and phonon-mediated relaxation in low-dimensional semiconductors and van der Waals materials [9,15,17]. Control of mesoscopic heat flow has enabled the realization of quantum-dot (QD) heat engines operating near thermodynamic efficiency limits [18], and advances in cryogenic calorimetry, bolometry, and noise thermometry [17,19,20]. Nevertheless, quantitative measurements of heat transport and electron-phonon interactions in semiconductor NWs remain challenging. A key experimental difficulty lies in the ability to inject well-defined heat into a nanoscale device while simultaneously performing local thermometry under thermal isolation.

In this work, we investigate the heat conduction and energy dissipation processes by using a hybrid semiconductor-superconductor architecture in which an epitaxial InAs NW hosts *insitu* grown QDs that work as a primary electronic thermometer. Superconducting contacts with negligible thermal conductance provide localized Joule heating while maintaining electrical control. By measuring the source and drain temperatures of the QD under steady-state heating, we map the spatial temperature profile along the wire. The

*Contact author: shaldar@iitk.ac.in
†Contact author: ville.maisi@ftf.lth.se

Published by the American Physical Society under the terms of the Creative Commons Attribution 4.0 International license. Further distribution of this work must maintain attribution to the author(s) and the published article's title, journal citation, and DOI. Funded by Bibsam.

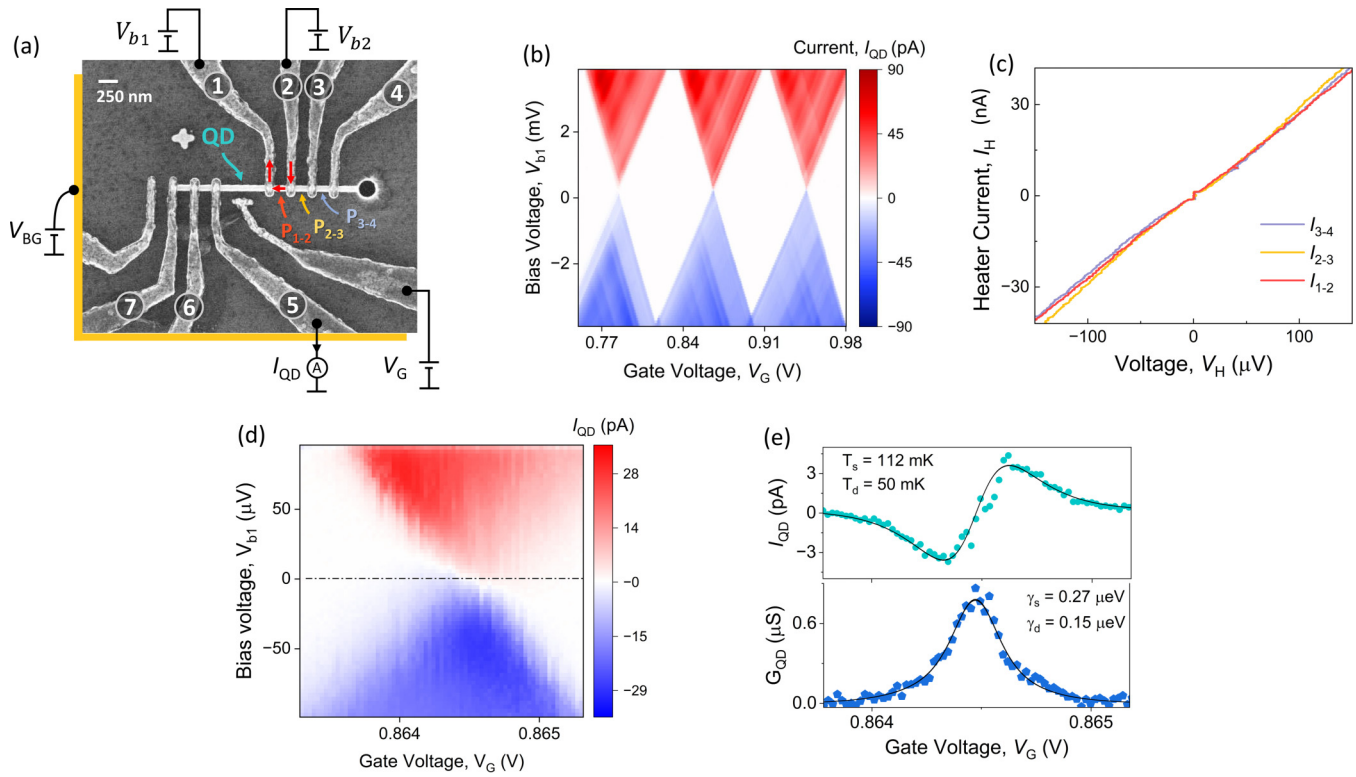


FIG. 1. (a) Scanning electron micrograph of the semiconductor-superconductor hybrid device showing the NW-QD with the superconducting contacts and measurement setup. The QD is located 1.3 μm away from the tip. The contacts are positioned 250 nm apart, which allows for localized Joule heating by passing current between different pairs of contacts. (b) The measured current through the QD as a function of bias voltage V_{b1} and side-gate voltage V_G, showing the standard Coulomb diamonds, and (c) current-bias voltage characteristics of the S-Sm-S contacts. (d) A zoomed-in image of the Coulomb peak, measured with 25 fW heating power applied to the 1-2 lead, and (e) the current and differential conductance data as a function of gate voltages at $V_{b1} = 0$. The solid lines are fits to Eq. (1).

resulting data are analyzed using a one-dimensional heat-transport model that incorporates both electronic diffusion and generalized $P \propto T^n$ electron-phonon cooling. This allows us to calculate key material and transport parameters, including the electron-phonon coupling strength, the dimensionality-dependent power-law exponent, and the characteristic thermal relaxation length.

II. EXPERIMENTAL DETAILS

Our hybrid device comprises a wurtzite InAs semiconductor NW, 70 nm in diameter, which is grown using the chemical beam epitaxy method [21]. During the NW growth, two ∼10-nm-long InP barriers were grown to confine electrons within a ∼100-nm-long InAs segment, forming a QD. The QD is located approximately 1.3 μm from the tip. As shown in Fig. 1(a), seven galvanic contacts, separated by ∼250 nm, are made on the NW using electron beam lithography (EBL) followed by thermal evaporation of 1 nm Ti/120 nm Al. These superconducting contacts are used to heat specific segments of the NW and measure electronic transport through the QD. Because at millikelvin temperatures the heat conductance of superconductors is very low, the electrons in the semiconductor are thermally isolated, such that the heat can only flow and be dissipated within the NW. Notably, during NW growth, an Au particle is used as a seed, which remains at the tip of the wire and forms a galvanic contact with the wire. To eliminate any unwanted heat dissipation by the Au particle, we remove it using an additional round of EBL followed by argon ion milling; the resulting dark spot at the tip of the NW is visible in Fig. 1(a). The device is fabricated on a degenerately doped Si substrate with a 200-nm-thick thermally grown SiO_2. The conducting substrate acts as a global back gate (V_{BG}), which helps in tuning the electrical conductivity of the entire wire and the QD. In addition, the side-gate voltage (V_G) controls the electrochemical potential (ε_N) of the QD directly. For the presented experiments, we use $V_{BG} = 4.5$ V and vary V_G. This back-gate voltage was required for sufficient source-drain current across the QD for thermometry, yet low enough to avoid lifetime broadening and excessive parasitic heat conduction through the QD. Measurements are performed in a dilution refrigerator with an electronic temperature, $T_e \approx 40$ mK.

Similar NWs have been used previously for thermoelectric devices and heat-transport measurements, both in the ballistic and diffusive regimes [5,22,23]. Transport experiments show that these wires have an electronic mean free path, $l_f \sim 100$ nm [5,24].

III. RESULTS AND DISCUSSION

We start by measuring the electronic transport properties of the QD in the absence of external heating. A bias voltage V_{b1} is applied to lead 1, and the resulting current I_{QD} across the QD is measured through lead 5, as illustrated in Fig. 1(a). All other

contacts are left electrically floating to avoid spurious Joule heating. Figure 1(b) shows the measured current as a function of V_{b1} and side-gate voltage V_G, showing Coulomb diamonds, characteristic of a QD. The gate voltage linearly tunes the electrochemical potential of the dot, $\varepsilon_N = \alpha_G V_G$, with a lever arm $\alpha_G = 49$ μeV/mV. From the periodicity of the Coulomb peaks, we determine the charging energy $E_c = 4$ meV. The nearly uniform peak separation indicates that the orbital level spacing is significantly smaller than E_c, consistent with the size of the dot in our experiment, $l_{QD} \sim 100$ nm.

The current-voltage characteristics of the superconductor-NW-superconductor segments used as heaters are shown in Fig. 1(c). All segments exhibit weak proximity-induced superconductivity with a critical current $I_c \approx 1.2$ nA, followed by an approximately linear resistive regime at higher bias. The reproducible and nearly identical behavior allows the contacts to be used as local Joule heaters with known input power.

A. Quantum-dot thermometry

To probe local electronic temperatures, we utilize the QD as a primary thermometer. When a heating voltage V_H is applied between a selected pair of contacts, the resulting temperature rise at the source and drain barriers of the QD, T_s and T_d, respectively, is calculated from the thermally broadened Coulomb peak. The QD operated in the thermally broadened regime has previously been used for thermometry [25,26]. In our configuration, the bias voltage applied to the QD is set by V_{b1}, while the heating power is determined by $V_H = V_{b2} - V_{b1}$ [Fig. 1(a)]. Figure 1(d) shows a representative charge-stability map obtained with a constant heating power of 25 fW applied between leads 1 and 2. The corresponding zero-bias current and conductance are shown in Fig. 1(e). To determine the zero-bias condition experimentally, we use the following criteria: (i) the broadening of the differential conductance G_{QD} in gate voltage V_G has the lowest value and (ii) the positive and negative thermocurrent maxima are nearly equal in magnitude [see Fig. 1(e)].

To estimate T_s and T_d, we fit the measured $I_{QD}(V_G)$ and $G_{QD}(V_G)$ using the Landauer-Büttiker formalism for a single-level QD,

$$I_{QD} = \frac{e}{h}\int \tau(E)[f_s(E) - f_d(E)]dE,$$
$$G_{QD} = \frac{e^2}{h}\int \tau(E)\left[\frac{df_s}{dE} - \frac{df_d}{dE}\right]dE, \quad (1)$$

where $\tau(E) = 2\Gamma\gamma/[\{E + \alpha_G e(V_G^0 - V_G)\}^2 + \gamma^2]$ is the energy-dependent transmission function with $\gamma = (\gamma_s + \gamma_d)/2$, $\Gamma = \gamma_s\gamma_d/(\gamma_s + \gamma_d)$, $f_{s(d)}$ are Fermi functions at temperatures $T_{s(d)}$, and V_G^0 denotes the gate voltage corresponding to the center of the zero-bias Coulomb peak.

The black solid curves in Fig. 1(e) show the representative fitted results using Eq. (1). We here calculate the following four parameters: temperatures T_s and T_d, and tunnel couplings γ_s and γ_d by fitting: (i) current maxima and their spread, and (ii) conductance peak height and width. The calculated parameter values are shown in the inset. We note that the energy of electrons at the base temperature $k_B T_e \sim 4$ μeV is an order of magnitude higher than the energy scale set by the tunnel couplings γ_s and γ_d (∼0.3 μeV). The device is intentionally tuned to the regime $\gamma_{s,d} \ll k_B T$, ensuring that the Coulomb peak shape is dominated by thermal broadening and thus sensitive to temperature.

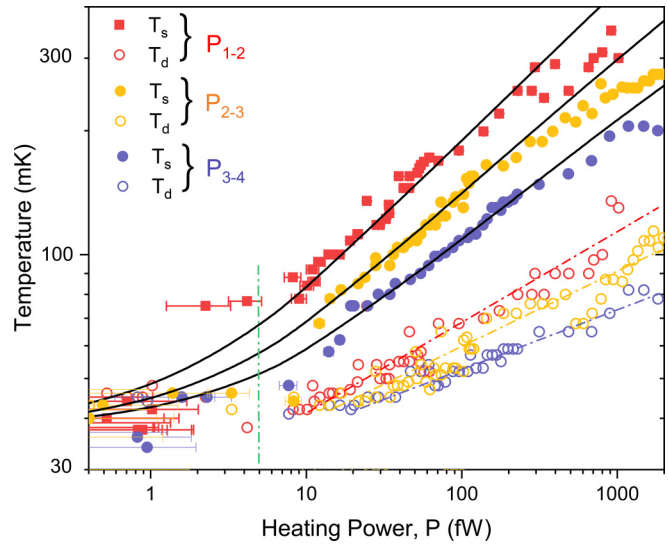


FIG. 2. Measured source (T_s) and drain (T_d) temperatures as a function of the heating power applied to the nanowire segments between leads 1-2, 2-3, and 3-4. The source electrode is on the heated side. Solid lines represent fits obtained using the one-dimensional heat-flow model of Eq. (6) with $\Sigma = 2 \times 10^9$ W/m^{3}K$^{2.6}$. The dashed curves are added as guides to the eye. The green dashed line marks the transition from the supercurrent regime to the Joule-heating regime in the S-Sm-S heaters.

Using this thermometry technique, we measure T_s and T_d as functions of the heating power applied to three different NW segments. The results are summarized in Fig. 2. When the heaters operate in the superconducting regime, no measurable temperature rise is observed, and both T_s and T_d remain at the base temperature of approximately 38 mK. Upon switching to the resistive regime, heating powers of ∼10 fW result in a measurable temperature increase. We note that, for a given input power, the measured T_s is highest when heat is injected closest to the QD and decreases as the heating location is moved farther away. This demonstrates the presence of longitudinal temperature gradients along the NW even under steady-state conditions. At higher powers, a small but measurable increase in T_d is also observed, indicating a weak heat leak through the QD during thermometry. This effect is analyzed quantitatively below.

Note that we have obtained a maximum heating power of $P = 1000$ fW with an applied bias voltage of $V_H \approx 60$ μV. The highest energy that an injected electron can have from this voltage source is thus 60 μeV. This maximum energy of the hot electrons in our experiment is a factor of 3 smaller than the superconducting gap of the aluminum leads ($\Delta \approx 180$ μeV) even with the highest applied V_H; as a result, the high-energy electrons cannot escape into the superconducting leads.

B. One-dimensional heat-transport model

To analyze the measured temperature profiles, we use a one-dimensional heat-flow model. For our NW with a

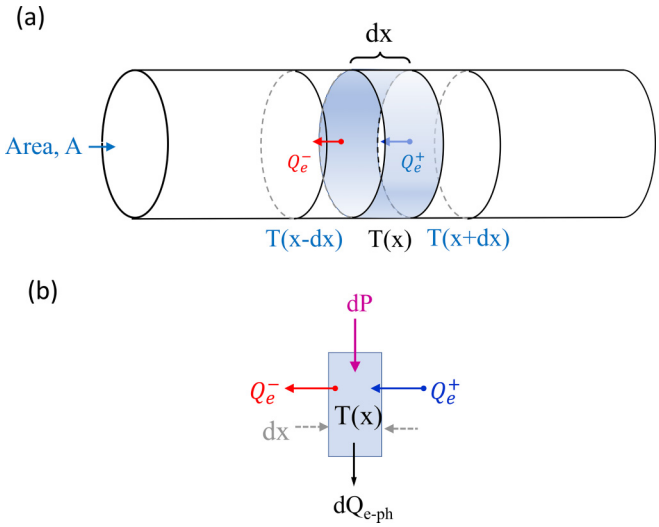


FIG. 3. (a) Schematic of a one-dimensional NW with cross-sectional area A, which consists of an elementary length dx, and the temperature at position x is denoted by $T(x)$. (b) The heat balance for an elementary volume showing the injected heating power as the sum of heat dissipation via electron-phonon interaction and heat conduction to the neighboring elements.

diameter of ∼70 nm, the electron and phonon modes are quantized in the transverse direction; therefore, a one-dimensional heat-transport model can be considered a good approximation [3,24]. We here discretize the NW into elementary lengths, dx, with $T(x)$ being the temperature at position x (see Fig. 3). The heat balance equation with the input heat dP to an elementary volume, $dv = A\,dx$, can be expressed as

$$dP = dQ_{\text{e-ph}} + dQ_c. \tag{2}$$

Here, $dQ_{\text{e-ph}}$ is the heat dissipation due to the electron-phonon interaction and dQ_c is the heat conduction along the NW. The first term of Eq. (2) can be written as

$$dQ_{\text{e-ph}} = \Sigma\, dv\left[T(x)^n - T_p^n\right], \tag{3}$$

where Σ is the electron-phonon coupling constant and T_p is the phonon temperature.

On the other hand, the net heat flow through an elementary volume is $dQ_c = (Q_e^- - Q_e^+)$, where Q_e^+ and Q_e^- are the heat entering and leaving the volume, respectively, as illustrated in Figs. 3(a) and 3(b). By assuming Wiedemann-Franz-like electrical heat conduction, this is given by

$$Q_e^{\pm} = \pm\frac{L\sigma}{2}\left[\frac{T(x \pm dx)^2 - T(x)^2}{dx}\right]A. \tag{4}$$

Here, the thermal conductivity is $\kappa_e(x) = L\sigma T(x)$, with σ being the electrical conductivity and $L = \xi L_0$, with the Lorenz number $L_0 = 2.44 \times 10^{-8}\ \text{W}\Omega/\text{K}^2$ and ξ is the effective Lorenz factor renormalization in our one-dimensional diffusive heat transport model that has the value $\xi = 1$ for the Wiedemann-Franz law.

Taylor expanding each term of Eq. (4) around x and neglecting higher-order terms, we have

$$dQ_c = -\left[\left\{\frac{dT(x)}{dx}\right\}^2 dx^2 + T(x)\frac{d^2T(x)}{dx^2}dx^2\right]\frac{L\sigma A}{dx}. \tag{5}$$

Finally, using Eqs. (2), (3), and (5), we can express the heat balance equation:

$$\frac{p}{L\sigma} = -\left[\left\{\frac{dT(x)}{dx}\right\}^2 + T(x)\frac{d^2T(x)}{dx^2}\right] + \frac{\Sigma}{L\sigma}[T(x)^n - T_p^n]. \tag{6}$$

Here, $p = dP/dv$ is the input heat power density.

C. Nanowire thermal properties

We fit the measured $T_s(P)$ in Fig. 2 using Eq. (6) with Σ, n, and the Lorenz factor ξ as free parameters. A single $T_s(P)$ curve provides two features: the overall magnitude and the exponent. The third constraint for fitting is obtained from the spatial dependence measured using heaters at different locations. Thus, all three datasets are fitted simultaneously with the same three free parameter values to obtain the values reliably and unambiguously. To fit the data, we solve the steady-state heat diffusion equation [Eq. (6)] for a parameter value set $\{\Sigma, n, \xi\}$ numerically. The numerical solver estimates the temperature profile $T(x)$ throughout the NW (see Supplemental Material [27]). We here used the electrical conductivity of the NW, $\sigma = 1.85 \times 10^4\ \Omega^{-1}\,\text{m}^{-1}$, calculated from the linear response regime of Fig. 1(c). The value of T_p is fixed to the bath temperature, $T_p = T_{\text{bath}} = 38$ mK, which is determined from the saturation of $T_s(P)$ in Fig. 2 as the applied heat $P \to 0$. Throughout our analysis, we assume that the NW phonons remain thermalized to the substrate phonon bath, as in Refs. [17,28,29], where the underlying substrate and the metal leads anchor the NW phonons to the bath.

The black curves in Fig. 2 show the fitted results with $n = 2.6 \pm 0.2$, $\Sigma = (2 \pm 0.2) \times 10^9\ \text{W/m}^3\text{K}^{2.6}$ and $\xi = 0.4 \pm 0.1$. A 60% reduction in the Lorentz factor shows a factor of 2 deviation from the Wiedemann-Franz law. The proximity effect, which induces partial superconductivity from the leads to the NW, is a likely reason for this suppressed heat conductance [30]. Comparing to other studies, Battisti *et al.* [7] recently investigated heat transport in two-dimensional InAs-on-insulator and reported electron-phonon coupling exponent $n = 6$ (compared to $n = 2.6$ in our case) and a coupling constant of $\Sigma \approx 4 \times 10^7\ \text{W/m}^3\,\text{K}^6$. At $T = 100$ mK, these values yield an estimated electron-phonon heat conductance per unit volume of $n\Sigma T^{n-1} \approx 2.4 \times 10^3\ \text{W/K}\,\text{m}^3$, which is approximately 5 orders of magnitude smaller than that obtained in our work ($1.3 \times 10^8\ \text{W/K}\,\text{m}^3$). Such differences in the reported parameter values may arise because of the different dimensionality, doping, confinement potentials, and scattering mechanisms between the two systems [31–33]. In particular, the charge accumulation at the surface of the InAs nanowire may influence the thermal transport properties as described in Ref. [15]. In another study, Ibabe *et al.* [34] investigated small segments of InAs NW sandwiched between superconducting leads and reported $n = 5$–6 with $\Sigma \approx 4.3 \times 10^9\ \text{W/m}^3\,\text{K}^6$,

which results in 3 orders of magnitude smaller electron-phonon heat conductance than in our work. One likely reason for their lower heat flow is a stronger suppression of electron-phonon coupling due to the proximity effect [35,36].

The value of n provides insight into the underlying electron–phonon coupling mechanism. In a clean low-dimensional conductor, the heat flow follows $Q_{\text{e-ph}} \propto T^{d+2}$, where d is the effective dimensionality [31]. For a one-dimensional nanowire ($d = 1$), the clean-limit prediction is $Q_{\text{e-ph}} \propto T^3$, close to our experimentally obtained exponent ($n = 2.6$). By contrast, in the disorder-dominated regime, $ql_{\text{ph}} \ll 1$, theory predicts $n \approx 4$ [32,37,38], where $q \sim k_B T/\hbar c_s$ is the phonon wave vector and l_{ph} is the phonon mean free path. Using $c_s \approx 4200$ m/s [7] and $l_{\text{ph}} \approx 250$ nm [39,40] for InAs NW, we estimate $ql_{\text{ph}} \approx 1.5$ at $T = 100$ mK. This places our device outside the disorder-dominated regime and supports a clean one-dimensional phonon subsystem that interacts with the NW electrons, consistent with the criterion $ql_{\text{ph}} \geqslant 1$ [32,37,38]. Furthermore, the slight reduction of the exponent below the ideal T^3 dependence may originate from the surface or interface scattering, which is known to renormalize the temperature scaling toward lower values [32,33].

Next, to realize the relative impact of electronic heat conduction and electron-phonon energy relaxation, we estimate the corresponding thermal conductance, G_c^t and $G_{\text{e-ph}}^t$. Using the Wiedemann-Franz relation, we calculate the thermal conductivity, $\kappa_e = \xi L_0 \sigma T = 1.8 \times 10^{-5}$ W m^{-1} K^{-1} at $T =$ 100 mK, and for a representative segment of length $l =$ 250 nm, the electronic thermal conductance $G_c^t = \kappa_e A/l =$ 2.8×10^{-13} W K^{-1}. In comparison, the thermal conductance due to electron-phonon coupling in the same segment is $G_{\text{e-ph}}^t = n\Sigma V T^{n-1} = 1.3 \times 10^{-13}$ W K^{-1} at 100 mK. The estimated G_c^t is more than a factor of 2 higher than $G_{\text{e-ph}}^t$ at this length scale, which implies that heat is removed more efficiently along the electronic channel than it is transferred to the phonon bath.

The above estimates also allow us to calculate the characteristic length scale at which electronic heat conduction and electron-phonon energy relaxation contribute equally to thermal transport. As the electronic thermal conductance scales as $G_c \propto l^{-1}$, whereas the electron-phonon thermal conductance scales as $G_{\text{e-ph}} \propto l$, equating the two yields

$$\ell_{\text{eq}} = \sqrt{\frac{\xi \sigma L_0}{n\Sigma T^{n-2}}}, \tag{7}$$

which for our NW is found to be $\ell_{\text{eq}} \approx 370$ nm at 100 mK. This sets the length scale over which both the thermal conductances compete. For segments shorter than ℓ_{eq}, electronic conduction dominates, whereas for longer segments electron-phonon relaxation determines the thermal response. The length of our NW is larger than ℓ_{eq}, which explains the spatial temperature variations observed experimentally.

D. Quantum-dot thermometer

We next turn to considering the QD thermometer and estimating the heat leak, P_L, through the dot during temperature measurements. We here use Eq. (6) to determine the value of

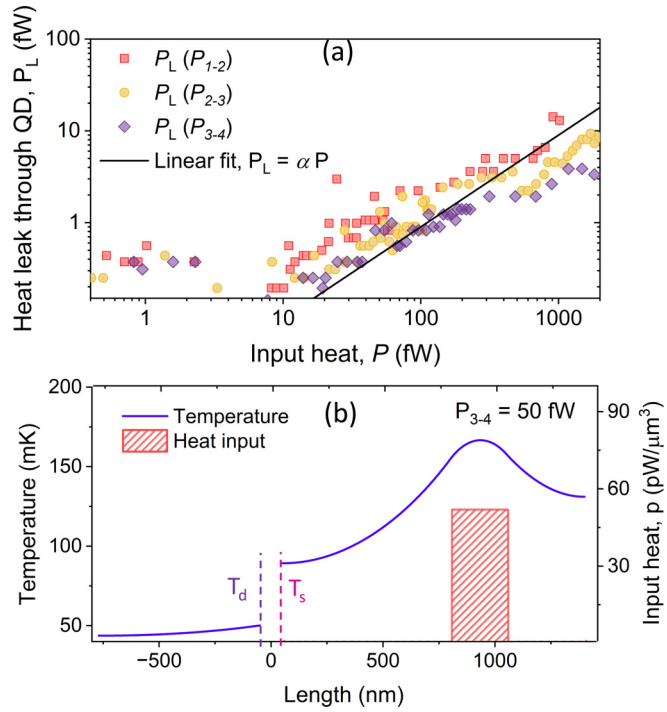


FIG. 4. (a) The amount of heat flowing through the QD as a function of the input heat to the NW, calculated from the measured drain temperature T_d. (b) Calculated temperature profile along the full length of the NW for an applied heating power of P_H=50 fW. The red bar indicates the heating power density p injected into the NW with leads 3 and 4.

P_L required to reproduce the measured drain-side temperature T_d shown in Fig. 2. We use the same parameter values Σ, n, and ξ that were determined for the source side. Figure 4 presents the calculated P_L as a function of the input heat. The black line in Fig. 4(a) shows the $P_L = \alpha P$ variation with $\alpha =$ 0.009. This confirms that the QD thermometer contributes less than 1% parasitic heat flow, demonstrating it as a minimally invasive probe for local electronic temperature measurement.

Using the measured source and drain temperatures across the 100-nm-long QD and the estimated heat leak P_L, we calculate the thermal conductance of the dot. For $T_s = 200$ mK, $T_d = 50$ mK, and $P_L = 1$ fW, we obtain $G_{\text{QD}}^t = P_L/(T_s - T_d) \approx 7 \times 10^{-15}$ W K^{-1}. The corresponding thermal conductivity is $\kappa_{\text{QD}} = G_{\text{QD}} l_{\text{QD}}/A \approx 2 \times 10^{-7}$ W m^{-1} K^{-1}. Under the same conditions, the electrical conductance is $\sigma_{\text{QD}} \approx$ 0.5 μS, calculated from the Coulomb peak, yielding an effective Lorenz number for the QD, $L = 2G_{\text{QD}}/\sigma_{\text{QD}}(T_s + T_d) \approx 1.1 \times 10^{-7}$ W Ω K^{-2}, about a factor of 4 higher than the Wiedemann-Franz value. We note that at the considered average temperature of $T \approx 125$ mK, the quantum of thermal conductance for a single ballistic channel is $G_q = \pi^2 k_B^2 T/3h = 1.2 \times 10^{-13}$ W K^{-1}. Thus, our measured G_{QD} is approximately 6% of this ballistic limit. This significant reduction is consistent with tunnel-limited transport in the Coulomb blockade regime. The suppression of electrical conductance and the observed enhancement of the Lorenz number suggest that the QD acts as an energy filter, selectively allowing high-energy carriers to contribute to heat transport [41].

E. Nanowire temperature profile

Combining all extracted parameters, we compute the full steady-state temperature profile along the NW for a representative heating power of 50 fW applied between contacts 3 and 4 [Fig. 4(b)]. The result shows the role of electronic heat transport and the heat relaxation length l_{eq} in determining temperature gradients along the NW.

We note that tuning the electrical conductivity of the NW by gate voltages may influence its thermal properties. However, a detailed study of this dependence is beyond the scope of the present work, as higher V_{BG} causes lifetime broadening of our QD thermometer, reducing its temperature sensitivity and increasing parasitic heat leakage.

IV. CONCLUSIONS

In conclusion, our measurements show a quantitative description of heat flow in an InAs nanowire in the clean one-dimensional limit for the phonon. The calculated electron-phonon exponent $n = 2.6 \pm 0.2$ indicates energy relaxation with clean one-dimensional coupling. The comparison of electronic heat conduction and phonon cooling shows a characteristic equilibration length $\ell_{\mathrm{eq}} \approx 370$ nm at 100 mK, which sets the length scale above which phonon-mediated thermal transport dominates over heat conduction. Measurement of the temperatures on both sides of the QD further allowed us to determine that less than 1% of the heat flows through the QD thermometer and that the thermometer exhibits a thermal conductance of only ∼6% of the thermal conductance quantum G_q. This high degree of thermal isolation ensures minimally invasive local thermometry by quantum dots. These results offer quantitative design rules for thermal management in nanowire-based quantum devices and demonstrate that InAs NW-QD can serve as sensitive, low-loss thermal links for hybrid quantum devices.

ACKNOWLEDGMENTS

We acknowledge fruitful discussions with Claes Thelander, Peter Samuelsson, Martin Leijnse, and Simon Wozny and financial support from the Knut and Alice Wallenberg Foundation through the Wallenberg Center for Quantum Technology (WACQT), the European Union (ERC, QPHOTON, 101087343), NanoLund, and the Swedish Research Council (Dnr 2019-04111 and Dnr 2023-04142).

Views and opinions expressed are those of the author(s) only and do not necessarily reflect those of the European Union or the European Research Council Executive Agency. Neither the European Union nor the granting authority can be held responsible for them.

DATA AVAILABILITY

The data that support the findings of this article are not publicly available. The data are available from the authors upon reasonable request.

[1] N. Mosso, U. Drechsler, F. Menges, P. Nirmalraj, S. Karg, H. Riel, and B. Gotsmann, Heat transport through atomic contacts, Nat. Nanotechnol. **12**, 430 (2017).

[2] J. P. Pekola, Towards quantum thermodynamics in electronic circuits, Nat. Phys. **11**, 118 (2015).

[3] I.-J. Chen, A. Burke, A. Svilans, H. Linke, and C. Thelander, Thermoelectric power factor limit of a 1D nanowire, Phys. Rev. Lett. **120**, 177703 (2018).

[4] X.-L. Shi, J. Zou, and Z.-G. Chen, Advanced thermoelectric design: From materials and structures to devices, Chem. Rev. **120**, 7399 (2020).

[5] M. Kumar, A. Nowzari, A. R. Persson, S. Jeppesen, A. Wacker, G. Bastard, R. L. Wallenberg, F. Capasso, V. F. Maisi, and L. Samuelson, Hot carrier nanowire transistors at the ballistic limit, Nano Lett. **24**, 7948 (2024).

[6] F. Giazotto, T. T. Heikkilä, A. Luukanen, A. M. Savin, and J. P. Pekola, Opportunities for mesoscopics in thermometry and refrigeration: Physics and applications, Rev. Mod. Phys. **78**, 217 (2006).

[7] S. Battisti, G. De Simoni, A. Braggio, A. Paghi, L. Sorba, and F. Giazotto, Extremely weak sub-kelvin electron–phonon coupling in InAs on insulator, Appl. Phys. Lett. **125**, 202601 (2024).

[8] G. Chen, Non-Fourier phonon heat conduction at the microscale and nanoscale, Nat. Rev. Phys. **3**, 555 (2021).

[9] D. Majidi, M. Josefsson, M. Kumar, M. Leijnse, L. Samuelson, H. Courtois, C. B. Winkelmann, and V. F. Maisi, Quantum confinement suppressing electronic heat flow below the Wiedemann–Franz law, Nano Lett. **22**, 630 (2022).

[10] D. L. Mickelsen, H. M. Carruzzo, S. N. Coppersmith, and C. C. Yu, Effects of temperature fluctuations on charge noise in quantum dot qubits, Phys. Rev. B **108**, 075303 (2023).

[11] B. Undseth, O. Pietx-Casas, E. Raymenants, M. Mehmandoost, M. T. Mądzik, S. G. J. Philips, S. L. de Snoo, D. J. Michalak, S. V. Amitonov, L. Tryputen, B. P. Wuetz, V. Fezzi, D. D. Esposti, A. Sammak, G. Scappucci, and L. M. K. Vandersypen, Hotter is easier: Unexpected temperature dependence of spin qubit frequencies, Phys. Rev. X **13**, 041015 (2023).

[12] D. Prete, P. A. Erdman, V. Demontis, V. Zannier, D. Ercolani, L. Sorba, F. Beltram, F. Rossella, F. Taddei, and S. Roddaro, Thermoelectric conversion at 30 K in InAs/InP nanowire quantum dots, Nano Lett. **19**, 3033 (2019).

[13] A. Hofmann, C. Karlewski, A. Heimes, C. Reichl, W. Wegscheider, G. Schön, K. Ensslin, T. Ihn, and V. F. Maisi, Phonon spectral density in a GaAs/AlGaAs double quantum dot, Phys. Rev. Res. **2**, 033230 (2020).

[14] J. Matthews, E. A. Hoffmann, C. Weber, A. Wacker, and H. Linke, Heat flow in InAs/InP heterostructure nanowires, Phys. Rev. B **86**, 174302 (2012).

[15] R. Wang, Y. Xiong, J. Sun, Y. Zhou, G. Song, G. Chen, and X. Liu, Remarkably suppressed lattice thermal conductivity of InAs nanowires by surface electron–phonon coupling, Appl. Phys. Lett. **127**, 022202 (2025).

[16] B. Kubala, J. König, and J. Pekola, Violation of the Wiedemann-Franz law in a single-electron transistor, Phys. Rev. Lett. **100**, 066801 (2008).

[17] B. Karimi, H. He, Y.-C. Chang, L. Wang, J. P. Pekola, R. Yakimova, N. Shetty, J. T. Peltonen, S. Lara-Avila, and S. Kubatkin, Electron-phonon coupling of epigraphene at millikelvin temperatures measured by quantum transport thermometry, Appl. Phys. Lett. **118**, 103102 (2021).

[18] M. Josefsson, A. Svilans, A. M. Burke, E. A. Hoffmann, S. Fahlvik, C. Thelander, M. Leijnse, and H. Linke, A quantum-dot heat engine operating close to the thermodynamic efficiency limits, Nat. Nanotechnol. **13**, 920 (2018).

[19] J. M. A. Chawner, S. Barraud, M. F. Gonzalez-Zalba, S. Holt, E. A. Laird, Yu. A. Pashkin, and J. R. Prance, Nongalvanic calibration and operation of a quantum dot thermometer, Phys. Rev. Appl. **15**, 034044 (2021).

[20] J. van der Heijden, Electron thermometry, arXiv:2403.16305.

[21] C. Fasth, A. Fuhrer, L. Samuelson, V. N. Golovach, and D. Loss, Direct measurement of the spin-orbit interaction in a two-electron InAs nanowire quantum dot, Phys. Rev. Lett. **98**, 266801 (2007).

[22] A. Svilans, M. Josefsson, A. M. Burke, S. Fahlvik, C. Thelander, H. Linke, and M. Leijnse, Thermoelectric characterization of the Kondo resonance in nanowire quantum dots, Phys. Rev. Lett. **121**, 206801 (2018).

[23] P. M. Wu, J. Gooth, X. Zianni, S. F. Svensson, J. G. Gluschke, K. A. Dick, C. Thelander, K. Nielsch, and H. Linke, Large thermoelectric power factor enhancement observed in InAs nanowires, Nano Lett. **13**, 4080 (2013).

[24] A. E. Hansen, M. T. Björk, C. Fasth, C. Thelander, and L. Samuelson, Spin relaxation in InAs nanowires studied by tunable weak antilocalization, Phys. Rev. B **71**, 205328 (2005).

[25] E. A. Hoffmann and H. Linke, Nanoscale thermometry with a quantum dot, J. Low Temp. Phys. **154**, 161 (2009).

[26] I. Ahmed, A. Chatterjee, S. Barraud, J. J. Morton, J. A. Haigh, and M. F. Gonzalez-Zalba, Primary thermometry of a single reservoir using cyclic electron tunneling to a quantum dot, Commun. Phys. **1**, 66 (2018).

[27] See Supplemental Material at http://link.aps.org/supplemental/10.1103/g2cs-pdcw for further information on the numerical fitting of the experimental data shown in Fig. 2 to determine the electron-phonon coupling constant Σ, the electron-phonon temperature exponent n, and the Lorenz factor renormalization ξ.

[28] J. T. Muhonen, A. O. Niskanen, M. Meschke, Y. A. Pashkin, J. S. Tsai, L. Sainiemi, S. Franssila, and J. P. Pekola, Electronic cooling of a submicron-sized metallic beam, Appl. Phys. Lett. **94**, 073101 (2009).

[29] J. T. Karvonen and I. J. Maasilta, Influence of phonon dimensionality on electron energy relaxation, Phys. Rev. Lett. **99**, 145503 (2007).

[30] J. T. Peltonen, P. Virtanen, M. Meschke, J. V. Koski, T. T. Heikkilä, and J. P. Pekola, Thermal conductance by the inverse proximity effect in a superconductor, Phys. Rev. Lett. **105**, 097004 (2010).

[31] N. A. Stepanov and M. A. Skvortsov, Electron-phonon relaxation in a model of a granular film, Phys. Rev. B **108**, 205415 (2023).

[32] A. Sergeev and V. Mitin, Electron-phonon interaction in disordered conductors: Static and vibrating scattering potentials, Phys. Rev. B **61**, 6041 (2000).

[33] R. Ceder, O. Agam, and Z. Ovadyahu, Nonohmicity and energy relaxation in diffusive two-dimensional metals, Phys. Rev. B **72**, 245104 (2005).

[34] Á. Ibabe, G. O. Steffensen, I. Casal, M. Gómez, T. Kanne, J. Nygård, A. Levy Yeyati, and E. J. H. Lee, Heat dissipation mechanisms in hybrid superconductor–semiconductor devices revealed by Joule spectroscopy, Nano Lett. **24**, 6488 (2024).

[35] D. Nikolić, D. M. Basko, and W. Belzig, Electron cooling by phonons in superconducting proximity structures, Phys. Rev. B **102**, 214514 (2020).

[36] T. T. Heikkilä and F. Giazotto, Phase sensitive electron-phonon coupling in a superconducting proximity structure, Phys. Rev. B **79**, 094514 (2009).

[37] B. L. Altshuler and A. G. Aronov, Electron–electron interaction in disordered conductors, in *Modern Problems in Condensed Matter Sciences*, edited by A. L. Efros and M. Pollak (Elsevier, New York, 1985), Vol. 10, pp. 1–153.

[38] J. Rammer and A. Schmid, Destruction of phase coherence by electron-phonon interactions in disordered conductors, Phys. Rev. B **34**, 1352 (1986).

[39] S. Dorsch, S. Fahlvik, and A. Burke, Characterization of electrostatically defined bottom-heated InAs nanowire quantum dot systems, New J. Phys. **23**, 125007 (2021).

[40] M. Y. Swinkels, M. R. van Delft, D. S. Oliveira, A. Cavalli, I. Zardo, R. W. van der Heijden, and E. P. A. M. Bakkers, Diameter dependence of the thermal conductivity of InAs nanowires, Nanotechnology **26**, 385401 (2015).

[41] B. Dutta, J. T. Peltonen, D. S. Antonenko, M. Meschke, M. A. Skvortsov, B. Kubala, J. König, C. B. Winkelmann, H. Courtois, and J. P. Pekola, Thermal conductance of a single-electron transistor, Phys. Rev. Lett. **119**, 077701 (2017).